

WAVEGUIDE EVANESCENT FIELD MICROSCOPIES FOR APPLICATION IN CELL- AND BACTERIA- BIOPHYSICS

Silvia Mittler

*Department of Physics and Astronomy, The University of Western Ontario, London, ON, N6G2P6, Canada
smittler@uwo.ca*

Keywords: Waveguide, Evanescent Illumination, Microscopy, WEEF and WEFS, Cells, Bacteria, Fluorescence, Scattering, Distance Mapping, Granularity, Application as a Sensor

Abstract: Two evanescent field microscopy technologies based on glass slab waveguides with permanent coupling gratings are presented: waveguide evanescent field fluorescence microscopy (WEEF) and waveguide evanescent field scattering microscopy (WEFS). The technologies are briefly described: the experimental setup is based on a conventional inverted microscope. A comparison to TIR and TIRF microscopy is given. The advantages of the waveguide method are clearly addressed. Various examples from for WEEF and WEFS microscopy are given. For WEEF: static distance mapping with a multimode waveguide, dynamic solubilisation studies of cell plasma membranes and the kinetic response of osteoblasts to trypsin. For WEFS: bacteria sterilization as well as cell adhesion and granularity studies. The latest development is a mass producible all-polymer-waveguide-chip to bring the technology to the interested scientific community.

1 INTRODUCTION

With the aim of developing new medical devices with direct tissue contact, drug delivery vehicles, and tissue engineering scaffolds, there has been increasing interest in recent years in the interactions of cells with both synthetic and natural biomaterials (Niu et al., 2005; Storrie et al., 2007). In particular, the study of the contact regions between a cell and its substratum is of considerable interest as its investigation delivers *inter alia* information about the cytocompatibility of the substratum - the affinity of cells towards that particular surface. Promotion or inhibition of cell adhesion to synthetic and natural biomaterials is often crucial to the proper function of a particular device. Some information concerning these interactions, e.g. the lateral location and the density of the adhesion sites, as well as their

relationship to the actin stress fiber system, part of the cell's cytoskeleton, can be inferred from fluorescence microscopy of immunolabeled molecules involved in adhesion; typically, vinculin, a protein located within the multi-protein complex that anchors the adhesion to the cytoskeleton inside the cell (Burmeister et al., 1998). These methods only deliver signals from the focus volume and no information about adhesion distances to the substratum. However, a direct and quantitative method to address the distance to the substratum is highly attractive. To address this need, different microscopic techniques based on electron microscopy (Chen and Singer, 1982) and optical means such as evanescent fields and interference techniques have been developed. Total internal reflection fluorescence (TIRF) (Burmeister et al., 1998; Burmeister et al., 1994), surface plasmon

resonance microscopy (SPRM) (Giebel et al., 1999), interference fluorescence microscopy (IRM) (Verschueren, 1985), fluorescence interference contrast (FLIC) microscopy (Braun and Fromherz, 1997) and combinations thereof (Burmeister et al., 1998; Atilgan and Ovrzyn, 2009) have been used to visualize and quantify these contacts. The contacts themselves had been discovered by interference reflection microscopy (IRM) in the 1970s (Abercrombie et al., 1971).

Bacteria, on the other hand, are the most metabolically diverse group of organisms found in all natural environments including air, water and soil. Bacteria commonly occur with food sources and are also found within and on our bodies. However, concerns exist over contamination of food, water, and air by pathogenic bacteria (Sapsford and Shiver-Lake, 2008) that can enter our bodies through ingestion, inhalation, cuts or lacerations (Pizarro-Cerda and Cossart, 2006). Therefore, there is an increasing interest in bacterial contamination and the need for anti-bacterial surfaces not only for application in the food industry but also for medical and hygienic purposes (Oliver, 2005). Over two million hospital-acquired cases of infection are reported annually in the USA, which lead to approximately 100,000 deaths annually and added nearly \$5 billion to U.S. healthcare costs (Madkour and Tew, 2008; Madkour et al., 2009). Contamination of medical devices (e.g., catheters and implants) has been attributed to 45% of these infections (Stamm, 1978). Bacterial contamination of any surface typically begins with the initial adhesion of only a few cells that can then develop into a more structurally cohesive biofilm in less than 24 hours when provided with suitable nutrient conditions sustaining metabolism and cell division (Hetrick and Schoenfisch, 2006). Therefore, a better understanding of bacterial adhesion to surfaces is important for technical surface development and in biomedical applications. However, the precise measurement of bacterial adhesion to surfaces are difficult and time consuming because bacterial cells typically occur on the micrometer-scale and their adhesion forces are generally low, typically 0.1–100 nN (Christianson, 2004). Recent studies on the detection of bacteria on surfaces have focused on similar imaging systems as with cells such as optical (Vasilev et al., 2009) and fluorescent microscopy (Pires et al., 2013) to image the bacteria themselves or luminescence measurement of the presence of cells by ATP (adenosine triphosphate) detection systems (Pera et al, 2010). Surface Plasmon Resonance (SPR) sensors (Taylor et al., 2008),

Nucleic Acid Detection (Schmidt et al, 2006), Optical Waveguide Lightmode Spectroscopy (Cooper et al., 2009), Optical Leaky Waveguide Sensors (Zourob et al., 2005), and Evanescent Mode Fiber Optic Sensors (Mazhorova et al., 2012) have also been applied in order to detect biochemical toxins as signatures of bacteria.

In conclusion, it is important to have methods which are able to investigate interfaces between a technical surface and a bacterium or cell.

In recent years, Total Internal Reflection Fluorescent (TIRF) microscopy has been demonstrated to be an effective method for studying cell-substrate interactions that occur at surfaces and interfaces. Using TIRF microscopy, the behaviour of various types of cells (Bauereiss et al., 2015; Liu, 2015) and bacteria (Smith et al., 2002, Vigeant et al., 2001) near surfaces has been characterized. Total Internal Reflection (TIR) Microscopy utilizes the basic technology of TIRF without any fluorescence dyes present in the sample by creating an optical contrast due to scattering (Byrne et al., 2008). Recent studies have also demonstrated the use of TIR for imaging microbial adhesion.

The waveguide evanescent field scattering technique was developed by Thoma et al. (Thoma et al., 1997; Thoma et al., 1998) for ultrathin technical structures on surfaces using ion exchanged waveguides. Later, Waveguide Evanescent Field Fluorescence (WEFF) microscopy was developed (Grandin et al., 2006; Agnarsson et al., 2009; Horvath et al. , 2005; Hassanzadeh et al., 2008) as a straightforward alternative to TIRF microscopy for imaging ultrathin films and cell-substrate interaction using fluorescence dyes located in the plasma membrane.

This paper will give an overview on biophysical applications of WEFF and WEFS microscopy on cells and bacteria and a short outlook on current developments to offer the methods to a broader user base.

2 EXPERIMENTAL

2.1 Waveguides

In this study home-fabricated, glass on fused silica, step-index slab waveguides or ion exchanged waveguides with holographic coupling gratings were used (Hassanzadeh and Mittler, 2011; Halfpap et al., 2012). The waveguides were reusable various times after thorough cleaning. A typical cleaning

procedure consisted of a submersion in 70% ethanol (Aldrich, Canada) with sonication (Branson 2510, Branson, USA) for 20 min and a blow-dry with nitrogen gas. To remove organic material, the dried samples were cleaned with Nano-Strip (KMG Chemicals Inc., Fremont, CA) at 80°C for 5 minutes. After the Nano-Strip application, the substrata were rinsed extensively in Milli-Q water and blown dry again.

2.2 Cell Culture

The osteoblastic cell line MC3T3-E1 (subclone 4, ATTC Catalog 3 CRL-2593) were cultured in flasks. The cleaned waveguides were sterilized for 3 hours by UV light. Growth medium was prepared from 17.8 ml α -minimum essential medium 1X (MEM; Gibco), 2 ml fetal bovine serum (FBS; Gibco) and 0.2 ml antibiotic-antimycotic solution 100X (Anti-Anti; Gibco). First the medium was aspirated from the cell culture flask. Dulbecco's phosphate-buffered saline 1X (PBS; Gibco) was added to wash the cell layer and aspirated subsequently. To detach the osteoblasts from the vessel wall, 5 ml trypsin-EDTA (0.05%, Gibco) was added and incubated at 37°C for 5 minutes. The culture was checked by phase-contrast microscopy to confirm that cells were released into the suspension. The trypsin was neutralized by adding 9 ml growth medium to the flask. The resulting cell suspension was diluted in growth medium to 10,000 cells per ml. Waveguides were placed in a Petri dish and 1 ml cell suspension per substrate was applied to the surfaces. Samples were then incubated for 24 h at 37°C, 100% humidity and 5% CO₂.

The waveguides were removed from the growth medium and excess medium was aspirated. Next, each waveguide was rinsed three times in PBS. For fixation, the waveguides with the cells on top were placed in a solution of 4% paraformaldehyde in PBS for 10 minutes at room temperature. Subsequently, samples were rinsed three times with PBS. To prevent desiccation, samples were kept in PBS until further treatment. A solution was prepared from 1.5 mg DiO in 1 ml dimethyl sulfoxide (DMSO) and heated to 37°C within 5 minutes. This mixture was sedimented for 5 minutes at 2000 rpm to separate solid residues. Ten μ l of this stock solution was dissolved in 1 ml growth medium to form the staining solution. The staining solution (200 μ l) was pipetted onto the corner of each waveguide and the waveguide gently agitated until all cells were covered with staining solution. The samples were

left in the solution for 20 minutes to incorporate the dye. Afterwards, the staining solution was drained and the waveguides were washed in PBS. For the removal of all unbound dye, the samples were immersed in PBS for 10 minutes and drained again. The entire wash cycle was repeated two more times. The waveguides were stored in PBS until performing WEFF microscopy. This procedure delivers fixed cells, cells that are "frozen" in their habitus (Lanier, 1981; Smit, 1974; Su, 2014) with the dye situated in the plasma membrane of the cells.

2.3 Bacteria Culture

Nitrobacter sp. 263 was cultured on R2A (Difco™) plates at room temperature (approximately 23°C) for two weeks. For each colonization experiment, bacteria from one R2A plate were removed and suspended in 1 ml of filter-sterilized (0.45 μ m pore-size) distilled deionized water to produce an aqueous bacterial suspension (with 10⁶ bacteria/ml). A separate stock solution of R2B (i.e., broth/liquid culture medium) was made by dissolving R2A in sterile, distilled, deionized water and filtering this solution to remove the agar constituent leaving the dissolved nutrients for bacterial growth.

Bacterial attachment to the waveguide surface was achieved by placing a 50 μ l aliquot of the bacterial suspension on top of the waveguide for one hour at 37°C. After bacteria attached to the surface, the waveguide was rinsed with sterile, distilled water and placed in a sterile Petri dish containing 20 ml of R2A and incubated for 24 hours at 37°C to allow the attached bacteria to grow. The samples were not agitated. After 24 hours incubation, the waveguides were examined using bright field microscopy to determine whether microcolonies had formed. Note that all images were taken of live cells in growth medium. Samples were then analysed using WEFS microscopy.

Sterilization experiments were performed. Separate bacteria suspensions of 10 ml (with 10⁶ bacteria/ml) were placed in a sterile, open glass dish and exposed in a low pressure collimate beam apparatus (LPCB) to induce sterilization (Hedrick et al., 2007; Kuo et al., 2003) at doses of 2, 4, 8, 14, 20 and 30 mJ/cm² by increasing time to produce different doses (Kuo et al., 2003). This mode of UV photon sterilization was chosen for its common use in industrial applications and its ability to disrupt and dimerize neighboring DNA bases (thymine

dimerization) that hinders bacterial growth but not viability (Berney et al., 2007; Durbej and Eriksson, 2002). Each ‘sterilized’ bacterial suspension, produced via the different dose exposures, was used in an identical colonization experiments as described above.

It is important to note that prior to the first and second colonization experiment, separate aliquots of all bacterial suspensions (1ml) were stained using BacLight™ (Invitrogen) Live-Dead stain and examined using fluorescence microscopy to confirm that the cells were viable.

2.4 WEFF and WEFS Microscope

The WEFF and WEFS microscope (Hassanzadeh et al., 2008) consisted of an inverted microscope (Zeiss, Oberkochen, Germany) with the waveguide being located on the sample stage (Fig.1). The specimen was positioned on top of the waveguide. An argon ion laser (35 LAP 341-200, CVI Melles Griot) operated at $\lambda = 488$ nm with a variable output power of 7- 126 mW or a HeNe laser with a wavelength of 543.8 nm (Research Electro-Optics, 0.5 mW) were used as light sources in WEFF and WEFS microscopy, respectively. A neutral density filter was placed directly behind the laser for power reduction, avoiding bleaching and overexposure. An iris aperture controlled the beam diameter.

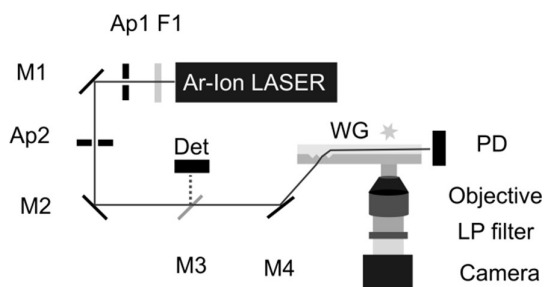


Figure 1: Schematic of WEFF microscope. Ap: aperture, F1: neutral density filter, M: mirror, WG: waveguide, PD: photo diode. For WEFS microscopy a HeNE laser was used and the LP filter omitted.

The laser beam was coupled into a chosen waveguide mode by a coupling grating located on the waveguide. In the case of WEFF microscopy, the undesired excitation wavelength was blocked with a long pass filter with a cut-off wavelength of $\lambda_{\text{cut-off}} =$

490 nm (3RD490LP, Omega Optics, Brattleboro, VT) which was fitted between the objective and the camera. The out-coupled intensity at the end of the waveguide was captured with a large active area photodiode (FDS1010, Thorlabs, Newton, NY) for determining the coupling efficiency when needed. A cooled CCD-camera (Persuit - XS 1.4 Diagnostic Instruments Inc., Sterling Heights, MI), controlled with SPOT 5 Basic (Spot Image Solutions, Sterling Heights, MI) was connected to a computer. Image data were exported for processing. Additionally, bright field microscopy images of the samples were captured with the same field of view/objective lens as the WEFF/WEFS microscopy images and processed with Image Pro Express (Media Cybernetics, Rockville, MD).

3 TIRF/TIR AND WEFF/WEFS COMPARISON

Both microscopy suits, TIRF/TIR and WEFF/WEFS, employ evanescent fields for sample illumination at the surface of a substrate which are produced by total internal reflection. In modern TIRF/TIR microscopes a laser beam is guided opto-mechanically within the microscope and the objective lens to allow a laser beam to undergo total internal reflection at a high refractive index substrate which carries the specimen and is located above the objective lens. Costly state-of-the art equipment and objective lenses with specially designed high magnification and high numerical aperture are necessary. Theoretically, all angles above the critical angle of TIR can be achieved in this way, giving the possibility to achieve different penetrations depth with different angles. This can be used to measure distances from the substrate surface (Truskey et al., 1992). Practically, the microscopes are set to particular angles, typically to receive a high quality TIRF or TIR image and a high quality epi-fluorescence or bright field image, respectively, taken with a transmitting beam.

On the other hand, operating a TIRF/TIR microscope manually can easily lead to a loss of the evanescent mode and to a full specimen exposure to the laser beam resulting in a damaged sample.

Reviewing the literature and in particular the use of TIRF microscopy for distance measurements shows that besides Burmeister’s excellent work in the middle of the 1990s (Burmeister et al., 1994) during the development phase of TIRF microscopy

only little has been published on exploiting different penetration depths.

TIR microscopy is performed identically but excluding the dye from the samples and the necessary filter sets. Scattered photons instead of fluorescence photons are collected. Bright field images are taken for comparison since epi-fluorescence is not possible. Little distance work has been published involving TIR microscopy (Smith et al., 2002). This is not surprising since the scattering intensities are hard to analyse because all refractive index fluctuations present in the evanescent field contribute to the signal and these are not necessarily controllable, in particular with living cultures producing extracellular matrix in the case of cells or extracellular polymeric substance (EPS) when imaging live bacteria.

In WEF/WEFS microscopy the resonances of the waveguide modes dictate the available evanescent fields and penetration depths. So the number of choices is limited by the number of modes propagating in the waveguide. In TIRF and TIR microscopy, the penetration depth of the evanescent field is limited to a maximum of ~ 200 nm, whereas a waveguides can produce penetrations depths from below 100 nm to over a μm by tuning the refractive index and thickness architecture of the core and cladding layers (Agnarsson et al., 2009). Planar waveguides also offer an extended illumination area over macroscopic dimensions only limited by the attenuation of the propagating waveguide mode.

In addition, the beam in WEF/WEFS can never escape the waveguide; therefore WEF and WEFS microscopies carry the intrinsic safety mechanism of avoidance of sample overexposure and damage.

In well characterized waveguides the evanescent fields and penetration depth are well known quantities and can be used for quantitative measurements (Hassanzadeh et al., 2009).

WEF and WEFS microscopy do not desire state-of-the-art microscopes or objective lenses. WEF and WEFS technologies are based on a few simple accessories and attachments to a standard inverted microscope. It is therefore straightforward to image the specimen in any magnification and field of view available due to standard long distance objective lenses by just turning the objective lens revolver without the necessity of beam stirring. Due to the evanescent field formation being taken care of by the substrate and completely independent from the entire microscope, different field of views or magnifications still deal with the same illumination

conditions allowing direct comparison of images or measurements after changing magnification.

Epi-fluorescence images can be achieved by simply enhancing the integration time of image acquisition. This is due to non-perfect waveguides: every waveguide scatters slightly and therefore supplies the 3D volume of the specimen with excitation or scattering photons.

Comparing TIRF and WEF images of the same samples has shown identical image information (Hassanzadeh et al., 2010). Both microscopy technology suits are diffraction limited, therefore the lateral resolution depends on the chosen laser wavelength and the highest possible magnification lens supported by the microscope used. The resolution in z-direction (perpendicular to the substrate) lies in both types of microscopes in the order of ~ 7 nm.

To achieve a wide use of WEF and WEFS microscopy in the interested research communities it is necessary to have simple access to and supply of inexpensive waveguide substrates. Therefore it is necessary to develop a mass producible waveguide-chip.

4 STATIC DISTANCE MAPPING WITH A MULTIMODE WAVEGUIDE

A waveguide with a thickness of 651 ± 2 nm and a refractive index of $n = 1.840 \pm 0.001$ was used for mapping the distances of the dye located in the plasma membrane of fixed osteoblasts. The volume above the waveguide was assumed to be water with a refractive index of 1.33 for simulating the evanescent fields. Two images taken with the TM_1 and TM_2 mode were used to calculate the dye distance map (Fleissner et al., 2015).

The WEF image in Fig.2 depicts four osteoblasts well spread and indicating the nuclei and some cell extensions. A false colour representation of Fig.2 can be found in (Fleissner et al., 2015). The dye distance map depicts lower distance grey values (dark) in the area of the cells from close to 0 to ~ 130 nm. In the unoccupied area, the unstained medium, where the raw data do not show fluorescence intensities, only noise is present. This is depicted as distances in the order of the penetration depth of the evanescent field: $\sim 160 \pm 40$ nm (noisy, dotted area). In addition, isolated spots in the no-sample area (outside the cells) are visible in black. These spots are correlated to un-physical distance

values below zero caused by microscopic damages of the waveguide. These un-physical distances should always be omitted in image interpretation. All four osteoblasts can be found in the distance map and show cell outlines similar to the cells depicted in the “epi-fluorescence” image. However, the lamellipodia and the thinly spread cell body are even clearer in the distance map. In Fig.2, the distance map does not depict any information about the nuclei. Not the entire cell body reached down very close to the surface, as expected. At some of the cells’ outer lines and at some extreme tips of the spread cells, small regions – only a few pixels in diameter – were found with distances of $\sim 10 - 25$ nm, typical of a focal adhesion (Chen and Singer, 1982; Tawil et al., 1993).

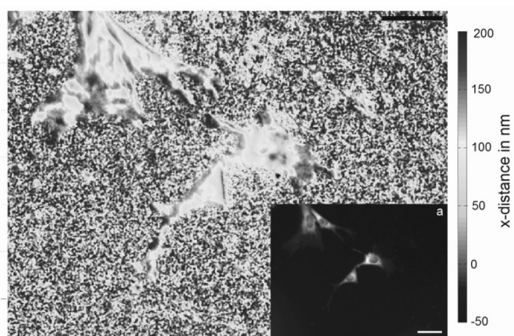


Figure 2: B/w representation of a dye distance map with four osteoblasts. The inset represents a WEFF image with increased integration time of the same field of view. The scale bar represents $50 \mu\text{m}$.

Twice line like accumulations of dense focal adhesions are found (very dark lines with distances around $10 - 25$ nm). Between the focal adhesions, there are regions in lighter dark grey depicting distances around $40 - 50$ nm as well as grey areas depicting distances around $70 - 80$ nm. Lamellipodia of the cells, which are very faintly seen in the epi-fluorescence images, are clearly visible in the distance map as thin spikes with a dark grey (possible focal adhesions or point contacts) or lighter dark grey (possible extracellular matrix contacts) center and bright grey to white surroundings (Chen and Singer, 1982).

Fig.3 (b in false colour representation in (Fleissner et al., 2015)) depicts one well spread osteoblast in epi-fluorescence WEFF and grey scale distance map imaging. Fig.4 shows the two z-cuts through the distance map: one randomly through the

cell, (Fig.4a) and one through an area including the smallest distances of the cell (Fig.4b).

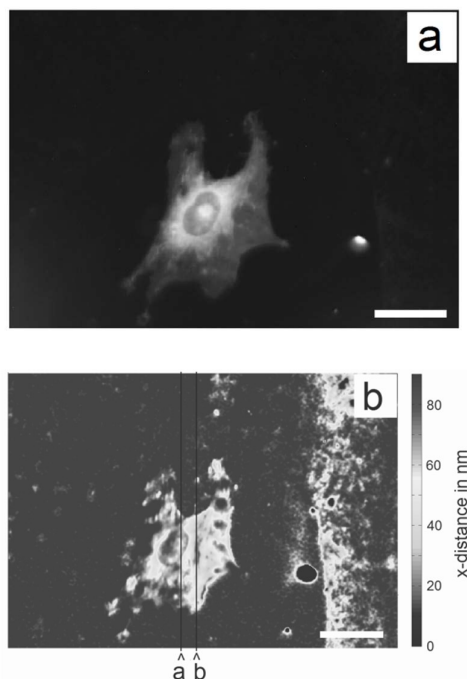


Figure 3: Single osteoblast. a) Epi-fluorescence WEFF image and b) b/w representation of the dye distance map with z-cuts. The scale bars represent $25 \mu\text{m}$.

The area outside the cell is nearly homogeneously dark grey. The existing noise level in the no-sample regions is clearly depicted in the z-cut data; it is the noisy data at an average distance of ~ 90 nm on both sides of the cell. The cell itself is shown by the depressions in the z-cuts with the dips indicating adhesions. The spreading of the cell is excellently depicted by the distance map. The cell is attached at all extreme spreading points, however not necessarily as focal adhesions since, distances above 40 nm and up to 50 nm, possible close contacts, are found. In the centre of the cell, focal adhesions are present.

The z-cuts show the position of the plasma membrane/dye location along the cut line in nm. For the random cut ‘a’, three “small” distances in the order of ~ 55 nm are found, as well as a couple of more bends towards the substratum with distances of $\sim 62 - 67$ nm. The maximum heights of the plasma membrane from the waveguide surfaces between the bends towards the substratum are found to be between 62 and 75 nm.

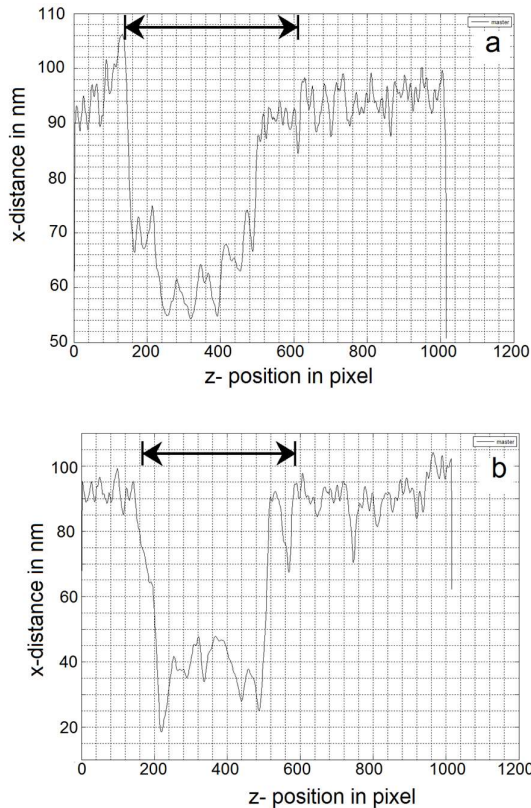


Figure 4: z-cut through cell at random position 'a' through cell at smallest distance locations at position 'b' in Fig.3. The cuts in Fig.3 from bottom to top are represented in Fig.4 from left to right. The scale bars represent 25 μ m. Arrows depict cell position.

In the z-cut 'b' through the small distance adhesions one focal adhesion at 18 nm is found as well as contacts with distances of 25 – 35 nm. The maximum heights of the plasma membrane from the waveguide surfaces in this case are 37 and 45 nm. The bending of the membrane towards the cytoplasm between these adhesions points is clearly depicted. The relative straight lines between the "maxima and minima" in the distance curve bear a resemblance to a stretched rubber band. One needs to keep in mind that the surface tension of the plasma membrane tries to minimize the surface area, trying to force the cell into a spherical shape. The adhesions are obvious biological disruptions of the physical effect of surface minimization.

With the current set-up it is not possible yet to do time laps distance mapping. An automatic motorized

mirror adjustment for M4 (Fig.1) needs to be implemented.

5 DYNAMIC SOLUBILISATION STUDIES OF CELL PLASMA MEMBRANES

Detergent-membrane interactions have been the subject of many studies (Ngassam et al., 2012). Functional membranes typically exist in the fluid state also called the liquid-disordered state. Due to difficulties of working with authentic cell membranes, simplified membrane models - such as supported lipid bilayers or liposome mimicking biological systems - have often been used to investigate detergent-membrane interactions (Ngassam et al., 2012). Model membranes were helpful in exploring the basic membrane functions. However, in comparison to a living cell, with integral and peripheral proteins, cholesterol molecules and oligosaccharides in and on their plasma membrane, artificial membrane models cannot mimic all aspects of plasma membrane function. In addition, studying the interaction between lipids and detergents in the form of vesicles (liposomes) or supported lipid bilayers has several other disadvantages. For example, in supported lipid bilayers, the quality of the deposited film plays a major role. The direct contact with the underlying substrate affects the bilayer's structure and fluidity, and blocks access of solutions to both sides of the membrane.

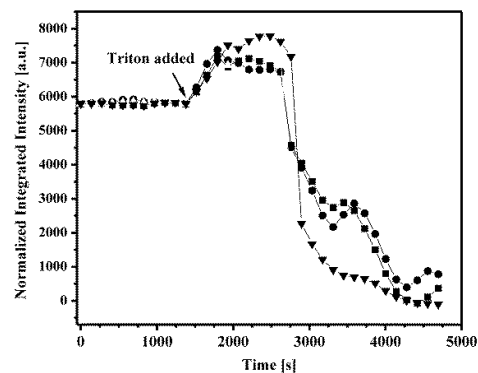


Figure 5: Normalized, integrated intensities of three cells versus time. Triton X-100 (0.013 w/w%) was added where indicated by the arrow.

The results of lipid-detergent interaction studies using bio-membrane models have been related to a three-stage model, which was described by Lichtenberg et al. (Lichtenberg et al., 1985). In stage I, with increasing detergent concentration, detergent incorporates into the bilayer. At this stage, solubilization does not occur, but the bilayer becomes saturated with detergent. At stage II, with further increase in detergent concentration, the bilayer starts to solubilise. Lipid vesicles saturated with detergent form and coexist with mixed micelles of lipid and detergent. At stage III, the entire membrane solubilises, and only mixed micelles exist (Csucs and Ramsden, 1998; Helenius and Simons, 1975).

Osteoblast were cultured on the waveguides and imaged alive with time laps WEFF microscopy. At a certain time Triton X-100 was added to the medium to start solubilisation. Fig.5 shows the normalized integrated intensity of the WEFF fluorescence signal of three example cells imaged with time.

In the absence of detergent, the integrated intensities are constant indicating negligible photo bleaching. In the presence of the detergent, three reproducible kinetic stages were found: i) an increase in fluorescence intensity, ii) a plateau, and iii) a decrease in intensity. Therefore, a comparison to or an adaption of the established three-stage model is possible. In stage I, the membrane takes up detergent and the concentration of detergent rises in the plasma membrane. The integrated fluorescence intensity increases due to suppression of fluorophore quenching by dilution of the dye with detergent (Silviu, 1992) in the cell membrane. In this stage, solubilisation does not occur. According to the model, stage I ends when the membrane becomes saturated with detergent. The end of stage I is seen in Fig.5 when the intensity increase ends and the plateau starts.

In stage II of artificial membrane solubilisation, the detergent-saturated lipid bilayer undergoes a structural transition and converts partially into lipid-detergent mixed micelles; however, these micelles are not yet mobile, but still incorporated in the membrane. Therefore, stage II is seen in our data as the plateau in which intensity remains constant as the dye is not leaving the evanescent field. At this time, the dye is still located either in the membrane or in formed micelles in unquenched conditions mixed with detergent.

During stage III, the micelles become mobile and leave the evanescent field, leading to a decrease in

integrated intensity. Individual micelles are too small to be seen with the WEFF microscope.

By changing the Triton X-100 concentration the duration of all three phases changed: the higher the detergent concentration the quicker the solubilisation stages (Hassanzadeh et al., 2012).

WEFF microscopy confirmed that living osteoblasts are solubilized in the same way as model membranes.

6 KINETIC RESPONSE OF OSTEOBLASTS TO TRYPSIN

Trypsin is a serine protease and cleaves peptide chains. Therefore, trypsin is used in laboratories to cleave proteins bonding the cultured cells to the dish, so that the cells can be suspended in fresh solution and transferred to fresh dishes.

Healthy osteoblast cells were grown directly on the waveguide and monitored with time laps WEFF microscopy. Trypsin was used at 0.05% and 0.02% concentration. Upon addition of 0.05% trypsin, the cells were lifted very fast and only individual focal adhesions could be imaged. However, with the lower concentration changes in cell morphology could be observed, such as cell retraction.

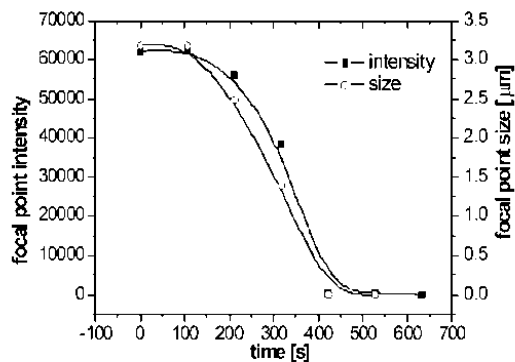


Figure 6: The impact of a 0.05% trypsin containing medium on an individual focal adhesion: intensity and size decrease with time. The lines are guides to the eye.

The quick disappearance of an individual adhesion point at the high trypsin concentration was examined. The focal adhesion point had the appearance of a bright circular dot. A series of images were taken with time and analyzed. Fig.6 depicts the kinetic behaviour of the adhesion point's disappearance, with respect of its integral intensity and size. Clearly both the size and the integral intensity of this individual focal adhesion point

decreased in an S-shaped curve and provided basically identical kinetic information about the detachment of the cell.

A sample was treated with 0.02% trypsin. The cells have shown cell retraction, and partly detached from the surface, leaving a black featureless evanescent image. After the trypsin treatment the medium was exchanged carefully to a trypsin-free environment. The imaging was continued. The osteoblasts, still alive, re-synthesise new adhesion proteins for the formation of new adhesion points. The kinetics of the adhesion process, until the cell population died and lost adhesion again, is depicted in Fig.7.

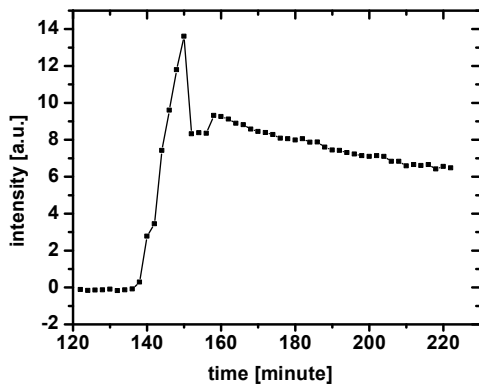


Figure 7: Integrated, intensity of 5 individual re-appearing adhesion points after exchanging a trypsin-containing medium at $t = 0$ to a trypsin-free medium.

7 BACTERIA STERILIZATION

Studies on the attachment of bacteria onto surfaces using WEFS microscopy detection is a quick method for investigations regarding bacterial sterilization treatment (Nahar et al., 2014). We hypothesized that non-potent, sterilized cells do not attach to surfaces and do not form microcolonies. Therefore, we have treated identical bacteria sample batches with different UV doses (2, 4, 8, 14, 20 and 30 mJ/cm^2). After the UV illumination the viability was measured. The UV illumination did not result in bacterial death. As a control, one sample was left without UV treatment. All bacteria illuminated with different UV doses and the control were cultured identically and examined using WEFS microscopy

after 24 h. Fig.7 shows a series of WEFS and bright field images of the control and UV treated bacteria.

The relative signal attributed to attached colonies and individual bacteria on the waveguide surface decreased as exposure to UV illumination was increased (Fig.8). It is significant to note that the highest dose of 30 mJ/cm^2 was not sufficient to completely prevent bacterial attachment.

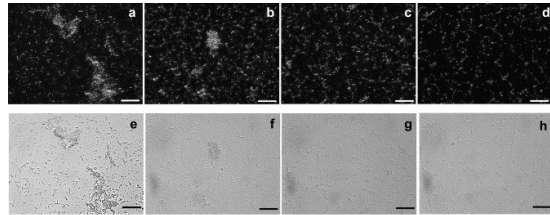


Figure 8: WEFS and bright field microscopy images of UV illuminated, sterilized bacteria after 24 h of culturing: a) and e) control: 0 mJ/cm^2 , b) and f) 8 mJ/cm^2 , c) and g) 20 mJ/cm^2 , d) and h) 30 mJ/cm^2 . The scale bars are 50 μm .

Both WEFS and bright field microscopy demonstrated that the highest dose resulted in the attachment of primarily individual bacteria, demonstrating that while attachment still occurred with increasing UV-dose, microcolony formation was prevented.

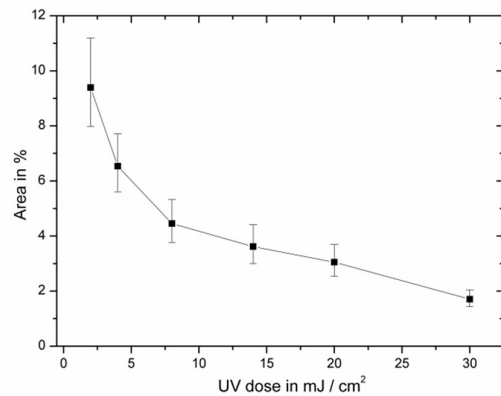


Figure 9: Percentage of occupied area of bacteria versus applied UV dose. The line is a guide to the eye only.

In order to yield quantitative data, a Matlab program was written to investigate the intensity distribution of each WEFS image and to calculate the percentage of area (i.e., pixels with signals above the defined threshold) occupied by bacteria (i.e.,

individual cells and cells comprising distinct colonies). Fig.9 shows the percentage of area on a sample occupied by bacteria versus the applied UV dose. Although the percentage of surface area with attached bacteria was decreasing exponentially, it did not reach zero. Bacteria were still attached to the waveguide surface despite the UV treatment.

A rough extrapolation of the exponential curve suggests that a dose of $>100 \text{ mJ/cm}^2$ would be required to completely hinder all bacterial attachment to the surface. If this had been a water sterilization experiment, at least a dose of 200 mJ/cm^2 (double safety) should be applied before release to the user.

8 CELL GRANULARITY AND ADHESIONS

Fixed osteoblasts were imaged with WEFS microscopy. Fig.10 shows a bright field image of a single osteoblast and the corresponding WEFS image. In the WEFS image the nucleus can be located: it is the dark area in the cell centre. In addition, the granular structures in the cell body and the adhesion sites at the cell outline are visible. Fig.10 indicates with the arrow the propagation direction of the waveguide mode. The cell's boundary first hit by the propagating light is shown very clear and with many adhesions points. The other three outer lines depict the adhesion points but not the complete cell boundary. At this chosen integration time the WEFS image depicts adhesions due to the evanescent illumination and the cell granularity due to 3D scattering of the waveguide.

Cell-substrate adhesions could be distinguished from scattering centres located further away from the substrate, the granularity of the cell, by varying the integration time. This is shown in Fig. 11.

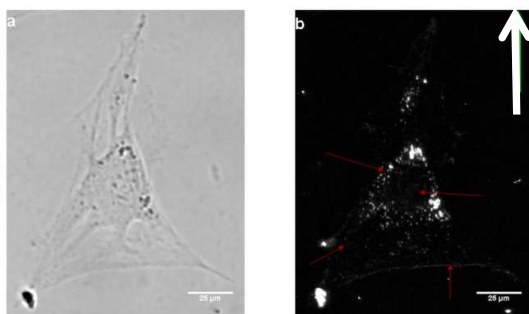


Figure 10: a) Bright field image and b) WEFS image of an osteoblast taken with an exposure time 3000 ms. The

green arrow indicates the direction of light propagation. The scale bars are $25 \mu\text{m}$.

With a very short integration time only a few spots appeared on the image in the areas where the cell was well spread. These spots are the cell's adhesions within the evanescent field. With increasing integration time, more and more features appeared, such as the cell nucleus area, the cells boundary and the cell granularity.

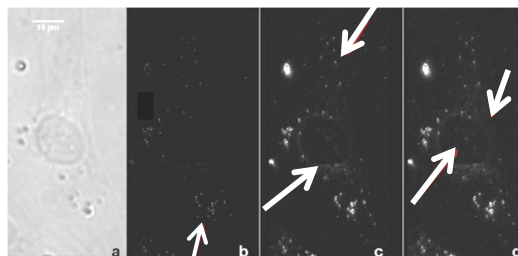


Figure 11: a) Bright field image of a single osteoblast and b)-d) corresponding WEFS images with integration times of 500 ms, 1000 ms and 1500 ms, respectively. The arrows point to the features mentioned in the text: a) adhesions, b) granularity and cell boundary, and c) nucleus and cell boundary.

These few experiments show that not necessarily fluorescence staining needs to be carried out for imaging focal adhesions and hence getting some cell-substratum interaction measures. As in WEFF microscopy larger integration times lead to 3D information of the cell.

Further detailed analysis, e.g. whether WEFS data are comparable with flow cytometry (scattering mode), need to be done.

9 MASS PRODUCIBLE WAVEGUIDE CHIPS

In order to allow WEFF and WEFS microscopy to be used by the interested communities, typically biophysics, biology, biochemistry and medical laboratories, the waveguide chips need to be available and at a reasonable cost. Mass production is the only way to achieve this. An all-polymer-waveguide chip with an imprinted coupling grating is one way to achieve this goal.

We have designed an all-polymer-waveguide chip on the basis of a PMMA substrate. The imprinting was performed into the PMMA with a home-fabricated silicon stamp and in a subsequent

step a polystyrene waveguide was spin coated on top.

Fig.11 shows SEM images of an imprinted grating with a periodicity of 670 nm and a depth of 200 nm.

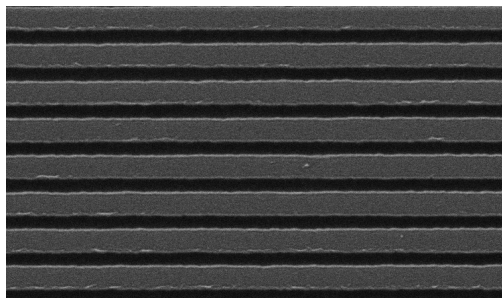


Figure 12: SEM image of a PMMA imprinted coupling grating. The periodicity is 670 nm.

First experiments with the all-polymer chips have produced promising WEFF imaging results. However, still development towards mass produced chips is necessary. The grating of Fig.11 was fabricated by imprinting one grating into one PMMA substrate. The imprinting and waveguide spinning procedure needs to be scaled up to do 16, 25, 36 or even 49 chips in parallel on one substrate with one imprinting procedure and a subsequent spin coating process.

10 CONCLUSIONS

We demonstrated a simple, cost effective and safe (sample safety) approach to perform TIRF and TIR microscopy on an existing inverted microscope by applying a slab waveguide as a sample substrate. No expensive, extremely low loss waveguides were needed. In contrary, the 3D scattering which is always present in non-sophisticated waveguides allowed to do epi-microscopy by simply enhancing the integration time.

We applied WEFF and WEFS to a variety of problems: from simple imaging of adhesions to quantitative investigations like distance maps and kinetic phenomena.

In order to spread the technology, the availability of mass produced, inexpensive waveguide-chips is necessary. The engineering towards this goal is on its way.

Both WEFF and WEFS microscopy will allow all kinds of interface and surface related imaging

and measurements. Both methods carry the possibility to also be used in sensor technology. Various options exist for using WEFF microscopy in sensing. One can think to operate a WEFF microscope with two simultaneously propagating modes at different wavelength for any kind of pump probe experiment. Or one can use a sensing scheme involving a Förster transfer changing the fluorescence yield upon binding of an analyte within the evanescent field and therefore detecting an image intensity change. WEFS microscopy is sensitive to any changes in the size or the density (refractive index) of the scattering entity. Recognition reactions on a surface could easily be detected by enhancing the scattering power by a gold nanoparticle (Klein, 2008) or by increasing the size of a scattering entity due to the binding.

Surface functionalization of the all-polymer-waveguide chip is possible with silane chemistry as -OH groups can easily be produced by oxygen plasma or UV ozone treatment (Kandeean et al., 2015).

ACKNOWLEDGEMENTS

Many co-workers, students, PhDs and colleagues are thanked for their contribution in the past, the present and the future for developing and applying WEFF and WEFS microscopy: Frank Thoma, John J. Armitage, Hugu Trembley, Michael Nietzsche, Abdollah Hassanzadeh, Rebecca Stuchburry, Sabiha Hacibekiroglu, Daniel Imruck, Christopher Halfpap, Michael Morawitz, Qamrun Nahar, Darryl K. Knight, Susanne Armstrong, Jeremia Shuster, Frederik Fleisser, Mihaela Stefan, Rony Sharon, Hong Hong Chen, Jeffrey S. Dixon, Stephen Sims, Kibret Mequanint, Uwe Langbein, Beth Gillies, Rene Harrison, Gordon Southam, Donglin Bai, Doug Hamilton, Cheryle Seguin, and Elisabeth Pruski.

REFERENCES

- Abercrombie, Heaysman, J.E., and Pegrum, S.M., 1971, *Exp. Cell Res.* **67**, 359 – 367.
- Agnarsson, B., Ingthorsson, S., Gudjonsson, T., and Leosson, K., 2009, *Optics Express* **17**, 5075-5082.
- Atilgan, E., and Ovrin, B., 2009, *Current Pharmaceutical Biotechnology* **10**, 508 – 514.
- Bauereiss, A., Welzel, O., Jung, Grosse-Holz, S. Leental, N., Lewczuk, P., Wenzel, E.M., Kornhuber, J. , and Groemer, T. W., 2015, *Traffic* **16**, 655-675.

- Berney, M., Hammes, F., Bosshard, F., Weilenmann, H.-U., and Egli, T., 2007, *Applied and Environmental Microbiology* **73**, 3283–3290.
- Braun, B., and Fromherz, P., 1997, *Applied Physics A-Materials Science & Processing* **65**, 341 – 348.
- Burmeister, J.S., Olivier, L.A., Reichert, W.M., and Truskey, G.A., 1998, *Biomaterials* **19**, 307 – 325.
- Burmeister, J.S., Truskey, G.A., and Reichert, W.M., 1994, *Journal of Microscopy-Oxford* **173**, 39 – 51.
- Burmeister, J.S., Truskey, G.A., Yarbough, J.L., and Reichert, W.M., 1994, *Biotechnological Progress* **10**, 26-31.
- Byrne, G. D., Pitter, M.C., Zhang, J., Falcone, F.H., Stolnik, S., and Somekh, M.G., 2008, *Journal of Microscopy*, 231, 168-179.
- Chen, W.T., and Singer, S.J., 1982, *Journal of Cell Biology* **95**, 205 - 222.
- Christianson, G.E., 2004, in *Molecular Adhesion and Its Applications, The Sticky Universe*, ed. Kevin Kendal, 275-303.
- Cooper, I.R., Meikle, S.T., Standen, G., Hanlon, G.W., and Santin, M., 2009, *J. Microbiol. Meth.* **78**, 40-44.
- Csucs, G., and Ramsden, J.J., 1998, *Biochimica et Biophysica Acta* **1369**, 304–308.
- Durbeej, B., and Eriksson, L.A., 2002, *Journal of Photochemistry and Photobiology A: Chemistry* **152**, 95–10.
- Fleissner, F., Morawitz, M., Dixon, S.J., Langbein, U., and Mittler, S., 2015, *Journal of Biophotonics* **8**, 826-837.
- Giebel, K.F., Bechinger, C., Herminghaus, S., Riedel, M., Leiderer, P., Weiland, U., and Bastmeyer, M., 1999, *Biophysical Journal* **76**, 509 – 516.
- Grandin, H.M., Städler, B., Textor, M., and Vörös, J., 2006, *Biosensors and Bioelectronics* **21**, 1476-1482.
- Halfpap, C., Morawitz, M., Peter, A., Detrez, N., Mittler, S., and Langbein, U., 2012, *DGAO Proceedings*, 0287-2012.
- Hassanzadeh, A., Nitsche, M., Mittler, S., Armstrong, S.J., Dixon, J., and Langbein, U., (2008) *Applied Physics Letters* **92**, 233503.
- Hassanzadeh, A., Armstrong, S., Dixon, S.J., and Mittler, S., 2009, *Applied Physics Letters* **94**, 033503.
- Hassanzadeh, A., Nitsche, M., Armstrong, S., Nabavi, N., Harrison, R., Dixon, S.J., Langbein, U., and Mittler, S., 2010, *Biomedical Optics* **15** 036018-1 - 036018-7.
- Hassanzadeh, A., and Mittler, S., 2011, *Optical Engineering* **50**, 071103.
- Hassanzadeh, A., Kan Ma, H., Dixon, S.J., and Mittler, S., 2012, *Biomedical Optics* **17**, 076025 1-7.
- Hedrick, R.P., Petri, B., McDowell, T.S., Mukkatira, K., and Sealey, L.J., 2007, *Diseases of Aquatic Organisms* **74**, 113-118.
- Helenius, A., and Simons, K., 1975, *Biochimica et Biophysica Acta* **415**, 29–79.
- Hetrick, E.M., and Schoenfish, M.H., 2006, *Chem. Soc. Rev.* **35**, 780-789.
- Horvath, R., Pedersen, H.C., Skivesen, N., Selmecezi, D., and Larsen, N.B., 2005, *Applied Physics Letters* **86**, 071101.
- Kandeeban, S., Paquette, J.A., Gilroy, J.B., and Mittler, S., 2015, CVD in press.
- Klein, A., Diploma Thesis, RheinMain University, Rüsselsheim, Germany, 2008.
- Kuo, J., Asce, M., Chen, C.-L., and Nellor, M., 2003, *Journal of Environmental Engineering* **129** 774-779.
- Lichtenberg, D., Robson, J., and Dennis, E.A., 1985, *Biochimica et Biophysica Acta* **821** 470-4778.
- Liu, X., Welf, E.S., and Haugh, J.M., 2015, *Journal of the Royal Society, Interface / The Royal Society* **12**, DOI:10.1098/rsif.2014.1412.
- Madkour, A.E., and Tew, G.N., 2008, *Polym. Intl.* **57**, 6.
- Madkour, A.E., Dabkowski, J.M., Nusslein, K., and Tew, G.N., 2009, *Langmuir* **25**, 1060-1067.
- Mazhorova, A., Markov, A., Ng, A., Chinnappan, R., Skorobogata, O., Zourob, M., and Skorobogatyi, M., 20012, *Opt. Express* **20**, 5344-5355.
- Lanier, L.L., and Warner, N.L., 1981, *Journal of Immunological Methods* **47**, 25-30.
- Nahar, Q., Fleissner, F., Shuster, J., Morawitz, M., Halfpap, C., Stefan, M., Southam, G., Langbein, U., and Mittler, S., 2014, *Journal of Biophotonics*, **7**, 542–551.
- Niu, X.F., Wang, Y.L., Luo, Y.L., Xin, J., and Li, Y.G. 2005. *Journal of Materials Science & Technology* **21**, 571- 576.
- Ngassam, V.N., Howland, M.C., Sapuri-Butti, A., Rosidi, N., Parikh, A.N., 2012., *Soft Matter* **8**, 3734-3738.
- Oliver, J.D., 2005, *J. Microbiol.* **43**, 93-100.
- Pera, N.P., Kouki, A., Haataja, S., Branderhorst, H.M., Liskamp, R.M.J., Visser, G.M., Finne, J., and Pieters, R.J., 2010, *Org. Biomol. Chem.* **8**, 2425-2429.
- Pires, L., Sachsenheimer, K., Kleintschek, T., Waldbaur, A., Schwartz, T., Rapp, B.E., 2013, *Biosensors and Bioelectronics* **47**, 157-163.
- Pizarro-Cerda, J., and Cossart, P., 2006, *Cell* **124**, 715-725.
- Sapsford, K.E., and Shiver-Lake, L.C., 2008, in Zourob, M., Elwary, S., and Turner, A.P.F. eds, *Principles of Bacterial Detection: Biosensors, Recognition Receptors and Microsystems*. Springer, 109-123.
- Schmidt, M., Hourfar, M.K., Nicol, S.-B., Wahl, A., Heck, J., Weis, C., Tonn, T., Spengler, H.-P., Montag, T., Seifried, E., Roth, W.K., 2006, *Transfusion* **46**, 1367-1373.
- Silvius, J.R., 1992, *Annual Review of Biophysics and Biomolecular Structure* **21**323-348.
- Smith, L.V., Tamm, L.K., and Ford, R.M., 2002, *Langmuir* **18**, 5247-5255.

- Smit, J.W., Meijer, C.J.L.M., Decay, F., and Feltkamp, T.M., 1974, *Journal of Immunological Methods* **6**, 93-98.
- Su, J.-W., Hsu, W.-C., Tjiu, J.-W., Chiang, C.-P., Huang, C.-W., and Sunga, K.-B., 2014, *Journal of Biomedical Optics* **19**, 075007.
- Stamm, W.E., 1978, *Annals of International Medicine* **89**, 764-769.
- Storrie, H., Guler, M.O., Abu-Amara, S.N., Volberg, T., Rao, M., Geiger, B., and Stupp, S.I., 2007, *Biomaterials* **28**, 4608 - 4618.
- Taylor, A.D., Ladd, J., Homolas, J., and Jang, S., 2008, in Zourob, M., Elwary, S., Turner, A., eds., *Principles of Bacterial Detection: Biosensors, Recognition Receptors and Microsystems XXXII* (Springer) 83-108.
- Tawil, N., Wilson, E., and Carbonetto, S., 1993, *Journal of Cell Biology* **120**, 261 – 271.
- Thoma, F., Langbein, U., Mittler-Neher, S., 1997, *Optics Communications* **134**, 16-20 (1997).
- Thoma, F., Armitage, J.J., Trembley, H., Menges, B., Langbein, U., and Mittler-Neher, S., 1998, *Proceedings of SPIE* **3414**, 242-249.
- Vasilev, K., Cook, J., and Griesser, H.J., 2009, *Expert Rev. Med. Devices* **6**, 553-567.
- Verschuere, H., 1984, *J Cell Sci* **75**, 279 – 301.
- Vigeant, M.A.S., Wagner, M., Tamm, L.K., and Ford, R.M., 2001, *Langmuir* **17**, 2235-2242.
- Truskey, G.A., Burmeister, J.S. Grapa, E., Reichert, W.M., 1992, *Journal of Cell Science* **103**, 491-499.
- Zourob, M., Mohr, S., Brown, B.J.T., Fielden, P.F., McDonnell, M.B., and Goddard, N.J., 2005, *Biosensors and Bioelectronics* **21**, 293-302.